ACS Macro Letters

Letter

Cite This: ACS Macro Lett. 2018, 7, 863−867

pubs.acs.org/macroletters

Nanoconfinement-Induced β-Phase Formation Inside Poly(vinylidene fluoride)-Based Block Copolymers

Niels L. Meereboer,[†] Ivan Terzić,[†] Sarah Saidi,[§] Daniel Hermida Merino,[‡] and Katja Loos*[,†]

[†]Macromolecular Chemistry and New Polymeric Materials, Zernike Institute for Advanced Materials, University of Groningen, Nijenborgh 4, 9747 AG Groningen, The Netherlands

[‡]ESRF - The European Synchrotron, CS 40220, Grenoble 38043 Cedex 9, France

[§]LMOPS, EA 4423, Université de Lorraine, CentraleSupelec Metz, 2 rue Edouard Belin, Metz, F-57070, France

Supporting Information

ABSTRACT: The electroactive properties of poly(vinylidene fluoride) (PVDF) are a direct consequence of its crystalline phases. Although poorly understood, nanostructuring PVDF in confined geometries can drastically change its crystallization behavior. Therefore, we synthesized a variety of PVDF-based triblock copolymers to gain a better understanding of the melt crystallization and explore how crystallization is affected by the morphology and chemical nature of the amorphous block. Differential scanning calorimetry, small-/wide-angle X-ray scattering, and transmission electron microscopy gave us excellent insights into the morphology and the corresponding crystalline phases. We find that crystallization of PVDF inside spherical nanodomains occurs via a homogeneous nucleation mechanism leading to a large undercooling and the formation of the thermodynamically favorable ferroelectric β-phase. On the contrary, when confined crystallization occurs inside a lamellar morphology, or in the case of breakout crystallization, a heterogeneous nucleation process leads to the formation of the nonferroelectric α-phase. Furthermore, favorable melt interactions between both blocks induce crystallization into the polar γ-phase at moderate cooling rates.

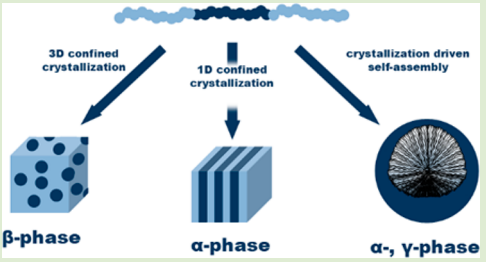

Ferroelectric polymers, next to organic semiconductors, play a major role in the development of future flexible organic devices (i.e., memory devices, sensors, transistors, photovoltaics, etc.) due to their ability to align dipoles in the direction of the applied electric field.[1] In this regard, poly(vinylidene fluoride) (PVDF) shows superior ferroelectric properties when crystallized in the β-phase compared to other ferroelectric polymers, such as odd-numbered nylons, even at elevated temperatures.[2,3] However, the nonferroelectric α-phase is predominant when PVDF is crystallized from the melt, whereas the crystallization into the more desirable β-phase is obtained when certain processing conditions are applied (i.e., ultrafast cooling, addition of nucleation agents, mechanical stretching, etc.).[4]

Melt crystallization of polymers in nanoconfined domains can drastically change the crystallization behavior, crystal orientation, and crystallinity and induce phase transformations and polymorphism.[5,6] For example, the crystal orientation of PVDF is changed from the on-edge α-phase to in-plane α-phase when the dimensions of laminated PVDF/poly(sulfone) are reduced from 225 to 28 nm.[7] Two-dimensional nanoconfinement is achieved when PVDF was melt-wetted into nanopores of ordered anodic aluminum oxide. The polymer still crystallizes in the nonferroelectric α-phase, although the growth of the *b*-axis of the crystal is limited to be parallel to the cylindrical axis.[8] Recently, Pan et al. have embedded PVDF nanoparticles in 180 nm polystyrene (PS) nanospheres followed by melt recrystallization.[9] Interestingly, the ferroelectric β-phase is obtained instead of the kinetically favorable α-phase. This is explained by a change of the crystallization mechanism from heterogeneous nucleation in zero, one, and two dimensions to homogeneous nucleation in three dimensions.[10,11]

The above-mentioned examples of confined crystallization of PVDF are all achieved via top-down approaches. Bottom-up approaches, such as block copolymer self-assembly, provide a cost-efficient method to make nanostructured ferroelectrics since no expensive equipment is required.[12] Using this approach, feature sizes beyond the limitations of top-down approaches are easily accessible by tuning the length scale of the block copolymers.[13] In addition, different types of confinement are realized by simply changing the ratio between the blocks, which makes block copolymer self-assembly an appealing method to study the crystallization of semicrystalline polymers inside nanodomains.[14] Crystallization from the melt within these nanodomains can give different outcomes.[5,15] First, breakout crystallization occurs when the interblock segregation strength between the distinct blocks is low, and crystallization-driven self-assembly will transform the melt morphology to a lamellar morphology with alternating

Received: May 31, 2018
Accepted: June 27, 2018
Published: July 2, 2018

DOI: 10.1021/acsmacrolett.8b00418
ACS Macro Lett. 2018, 7, 863−867

Table 1. Molecular Characteristics and Crystallinity of the Block Copolymers

polymer	M_n (kg/mol)[a]	$Đ$[b]	$w_{amorphous\ block}$[c]	w_{PVDF}[c]	$v_{amorphous\ block}$[d]	v_{PVDF}[d]	X_c (%)[e]
PVDF	12.6[f]	1.53[f]	0	1	0	1	49
P*t*BA$_{0.3}$-*b*-PVDF$_{0.4}$-*b*-P*t*BA$_{0.3}$	30.0[g]	1.56[h]	0.60	0.40	0.72	0.28	46
P2VP$_{0.27}$-*b*-PVDF$_{0.46}$-*b*-P2VP$_{0.27}$	28.0[g]	1.96[h]	0.55	0.45	0.66	0.34	15
P2VP$_{0.17}$-*b*-PVDF$_{0.66}$-*b*-P2VP$_{0.17}$	19.4[g]	n.d.	0.35	0.65	0.44	0.56	37
P2VP$_{0.06}$-*b*-PVDF$_{0.88}$-*b*-P2VP$_{0.06}$	14.3[g]	1.53[h]	0.12	0.88	0.18	0.82	37

[a]Number-average molecular weight (M_n). [b]Dispersity ($Đ = M_w/M_n$). [c]The weight fractions were determined by ^{1}H NMR spectroscopy. [d]The volume fractions were calculated using the weight fractions and the density of PtBA (1.05 g/cm^3), P2VP (1.14 g/cm^3), and PVDF (1.78 g/cm^3). [e]The degree of crystallinity of the PVDF block was determined from the weight fractions, the crystallization exotherm obtained from DSC, and the theoretical 100% melting enthalpy of α-phase PVDF (104.5 J/g) and β-phase PVDF (219.7 J/g).[23] [f]The molecular weight characteristics of PVDF were calculated using GPC with DMF (0.01 M LiBr) as eluent and monodisperse PMMA standards. [g]The block copolymer molecular weights were calculated using the M_n of PVDF and weight fractions of the distinct blocks. [h]The $Đ$ of the block copolymers is determined using GPC with THF as eluent and monodisperse PS standards.

crystalline and amorphous domains.[16] Second, confined crystallization can occur if the interblock segregation strength is sufficiently high. In this case, the melt morphology will be preserved after crystallization inside the nanosized domains.[5,10]

Recently, we have shown that a wide variety of PVDF-based triblock copolymers can be prepared via a copper(I)-catalyzed azide−alkyne cycloaddition (CuAAC) reaction.[17,18] In order to study the effect of the crystallization mode on the crystalline phase in PVDF block copolymers, we used various PVDF-based triblock copolymers with different weight ratios compared to the PVDF block. As displayed in Scheme S1 (see Supporting Information), alkyne-terminated telechelic was prepared via free radical polymerization. Azide-terminated poly(2-vinylpyridine) (P2VP) and poly(*t*-butyl acrylate) (P*t*BA) were prepared via reversible addition−fragmentation chain transfer (RAFT) polymerization. Subsequently, a CuAAC reaction was performed to obtain the ABA triblock copolymers, wherein an excess of either P2VP or P*t*BA was added to ensure complete conversion of the alkyne moieties. Excess of P2VP or P*t*BA was washed away with a selective solvent after the reaction. Full conversion of the alkyne-functionalized PVDF was confirmed with a downfield shift of the aromatic protons originating from the initiator fragments and the disappearance of the alkyne proton in the ^{1}H NMR spectrum (Figure S1). Size exclusion chromatography was used to confirm complete removal of the homopolymers and thus the successful formation of the triblock copolymers. The PVDF-based triblock copolymers are listed in Table 1. The PVDF molecular weight is calculated according to PMMA standards in GPC, from where the block copolymer molecular weights are determined using the molecular weight ratios obtained via ^{1}H NMR spectroscopy. The triblock copolymer films were cast from dimethylformamide (DMF) at 45 °C. After complete evaporation of DMF, the block copolymers were heated to the melt and cooled down with 10 °C/min in order to study their morphology and crystallization behavior.

Figures 1a, 1b, and 1c show the small-angle X-ray scattering (SAXS) profiles in the melt and after crystallization, the transmission electron microscopy (TEM) image, and the wide-angle X-ray scattering (WAXS) profile for P2VP$_{0.27}$-*b*-PVDF$_{0.46}$-*b*-P2VP$_{0.27}$ at room temperature, respectively.[19,20] The SAXS profile reveals only one peak (q = 0.184 nm^{-1}, d = 34 nm), which is insufficient to conclude anything about the melt morphology. However, based on the TEM image, we suggest that a disordered spherical morphology is obtained, wherein PVDF (dark domains) is embedded in a P2VP (light domains) matrix, with an interdomain distance that is in

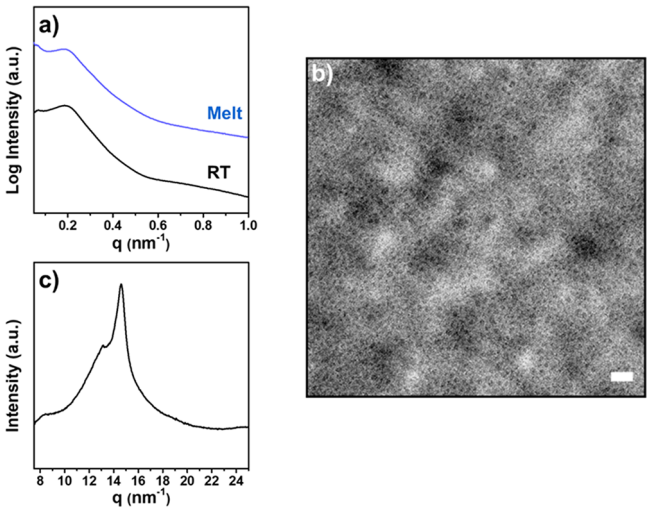

Figure 1. SAXS profiles (a), TEM image (b), and WAXS profile (c) for P2VP$_{0.27}$-*b*-PVDF$_{0.46}$-*b*-P2VP$_{0.27}$. Scale bar corresponds to 100 nm.

agreement with the one calculated from SAXS. In contrast to our observations, theory predicts the formation of cylinders based on the volume fraction of both blocks, whereas experimental observations by Widin et al. show a possible nanosphere formation in this composition range.[14,21] Indeed, a higher dispersity of the minority block may cause a phase shift from cylinders to spheres since stretching of the majority block overcomes the conformational entropy loss when a curved interface is formed.[22] The relatively high dispersity of the PVDF block prevents the appearance of higher-order scattering maxima in the SAXS profile.[14] However, no change of shape and position of the SAXS signal is observed after cooling to room temperature, which demonstrates that P2VP$_{0.27}$-*b*-PVDF$_{0.46}$-*b*-P2VP$_{0.27}$ can be used to confine the crystallization of PVDF.

Differential scanning calorimetry (DSC) was performed to gain better insights into the crystallization mechanism. The thermograms of PVDF and the triblock copolymers, depicted in Figure 2, show that crystallization of P2VP$_{0.27}$-*b*-PVDF$_{0.46}$-*b*-P2VP$_{0.27}$ takes place at lower temperatures compared to the parent homopolymer. The large number of nuclei that is needed for the crystallization inside the spherical domains results in a homogeneous nucleation process since the number of spheres outnumbers the impurities that can initiate crystallization by several orders of magnitude.[5] In addition, vitrification of the P2VP matrix upon cooling is observed before crystallization of PVDF, which leads to a low degree of

DOI: 10.1021/acsmacrolett.8b00418
ACS Macro Lett. 2018, 7, 863−867

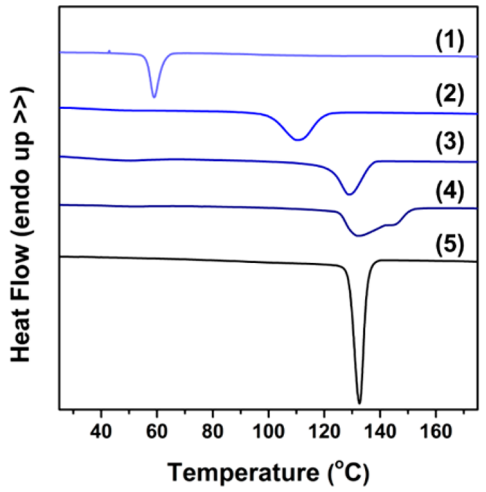

Figure 2. DSC cooling scans from the melt for $P2VP_{0.27}$-*b*-$PVDF_{0.46}$-*b*-$P2VP_{0.27}$ (1) showing confined crystallization in spheres, $PtBA_{0.3}$-*b*-$PVDF_{0.4}$-*b*-$PtBA_{0.3}$ (2) showing breakout crystallization, $P2VP_{0.17}$-*b*-$PVDF_{0.66}$-*b*-$P2VP_{0.17}$ (3) showing confined crystallization in lamellae, $P2VP_{0.06}$-*b*-$PVDF_{0.88}$-*b*-$P2VP_{0.06}$ (4) showing crystallization-driven self-assembly, and pure PVDF (5).

crystallinity due to a strongly reduced mobility of the polymer chains in the early stage of crystallization.

Strikingly, the WAXS profile of $P2VP_{0.27}$-*b*-$PVDF_{0.46}$-*b*-$P2VP_{0.27}$ reveals that nanoconfinement has a profound effect on the crystallization of PVDF, inducing the formation of the ferroelectric β-phase. The scattering peak in the WAXS profile of the (110/200) crystal planes at q = 14.6 nm^{-1} is easy to distinguish from the peaks corresponding to other crystalline phases. In addition, the Fourier transform infrared (FTIR) spectrum (Figure S3) shows the absorption bands at 840 and 1279 cm^{-1} confirming the all-trans conformation of the polymer chains inside the crystal.[4] On the contrary, pure PVDF crystallizes from the melt in the α-phase at moderate crystallization rates.[24] Gregorio and Cestari demonstrated that the maximum rate of crystallization for the β-phase happens at 60 °C, whereas a maximum crystallization rate for the α-phase occurs at 130 °C.[25] This suggests that at lower temperatures the thermodynamically favorable crystalline structure is formed probably as a result of a higher packing density of the β-phase compared to the α-phase, which reduces the free energy of the system by less steric interaction.[26] By confining the crystallization in spherical domains and forcing crystallization via a homogeneous nucleation mechanism, we managed to shift the crystallization temperature to values at which a maximum crystallization rate of the β-phase is observed. Similar results were obtained when PVDF nanoparticles were embedded in polystyrene nanospheres and subsequently recrystallized from the melt or via ultrafast quenching of PVDF films, which leads to a low crystallization temperature (around 30 °C) and the formation of the β-phase.[9,27,28] In contrast to these complicated procedures, confined crystallization of PVDF after block copolymer self-assembly proves to be an easy method to obtain the β-phase.

To verify that the β-phase formation is a consequence of the strong reduction in crystallization temperature, we prepared a $PtBA_{0.3}$-*b*-$PVDF_{0.4}$-*b*-$PtBA_{0.3}$ triblock copolymer with a similar volume fraction of P*t*BA as in $P2VP_{0.27}$-*b*-$PVDF_{0.46}$-*b*-$P2VP_{0.27}$. A phase-separated melt is formed after melting of PVDF, and surprisingly the first-order scattering maxima were retained at the same position after the room temperature morphology is obtained (Figure S5a). Probably, the bulky *tert*-butyl groups of P*t*BA disrupt hydrogen bonding between the carbonyl groups of *t*BA and the hydrogen atoms of VDF, causing microphase separation in the melt.[29] However, the glass transition temperature of P*t*BA was too low to preserve crystallization inside the melt morphology. As a result, breakout crystallization completely erases the melt structure, making an alternating crystalline−amorphous morphology as depicted in the TEM image (Figure S5b). The difference between the two crystallization modes, confined and breakout crystallization, is better observed under a polarized optical microscope (POM). In $PtBA_{0.3}$-*b*-$PVDF_{0.4}$-*b*-$PtBA_{0.3}$, we observe a clear birefringence pattern showing the spherulitic superstructure, whereas the absence of macroscopic crystallization results in an optically homogeneous POM image of $P2VP_{0.27}$-*b*-$PVDF_{0.46}$-*b*-$P2VP_{0.27}$ (Figure S4).[30]

The high molecular weight of the P*t*BA block significantly reduces the crystallization temperature from 132.5 to 110.5 °C. However, the crystallization temperature is much higher than for the crystallization of PVDF inside spherical nanodomains. Moreover, the degree of crystallinity of the $PtBA_{0.3}$-*b*-$PVDF_{0.4}$-*b*-$PtBA_{0.3}$ triblock copolymer is almost similar to its parent PVDF homopolymer indicating that breakout crystallization, especially regarding the high volume fraction of P*t*BA, occurred. As above-mentioned, at high temperatures the kinetically favorable α-phase is formed, which is in excellent agreement with the WAXS data depicted in Figure S5c. The peak positions q at 12.6, 13.1, 14.2, and 18.8 nm^{-1} from the WAXS profile of this block copolymer correspond to the (100), (020), (110), and (021) crystal planes of the alpha crystals, respectively.[4] Moreover, the absorption bands in the FTIR spectrum (Figure S3) that belong exclusively to the α phase are clearly visible. As already explained, the crystallization rate for α-phase formation at 110.5 °C is still high, whereas the rate of crystallization for the β-phase is practically zero.[25] Furthermore, crystallization of PVDF during breakout is barely hampered, resulting in a degree of crystallinity that closely matches pure PVDF, which is completely different from $P2VP_{0.27}$-*b*-$PVDF_{0.46}$-*b*-$P2VP_{0.27}$ where three-dimensional confinement reduces the degree of crystallinity to 15% (Table 1).

In order to examine the influence of confinement type on PVDF crystallization, we synthesized a $P2VP_{0.17}$-*b*-$PVDF_{0.66}$-*b*-$P2VP_{0.17}$ block copolymer with a similar volume fraction of both blocks. From the TEM image (Figure 3c) of the block copolymer, we observe a symmetrical lamellar morphology, whereas the SAXS profile in the molten state shows two signals with a ratio $1q$:$2q$ (q = 0.261 nm^{-1}, d = 24 nm). Due to the absence of more higher-order scattering maxima, the lamellar morphology is concluded based on TEM interpretations. The domain spacings calculated from the SAXS profile and observed from TEM were in good accordance. The fact that the position of the first-order peak did not change upon cooling to room temperature indicates that the lamellar morphology from the melt was retained upon PVDF crystallization due to the strong interblock segregation between PVDF and P2VP. Moreover, the POM image of the block copolymer did not show birefringence (Figure S4), confirming the confined crystallization (Table 1).

Crystallization within alternating lamellar domains occurred solely in the α-phase as shown in the WAXS (Figure 3b) and FTIR spectra (Figure S3), which can be elucidated by analyzing the thermal behavior. In the DSC thermogram we

DOI: 10.1021/acsmacrolett.8b00418
ACS Macro Lett. 2018, 7, 863−867

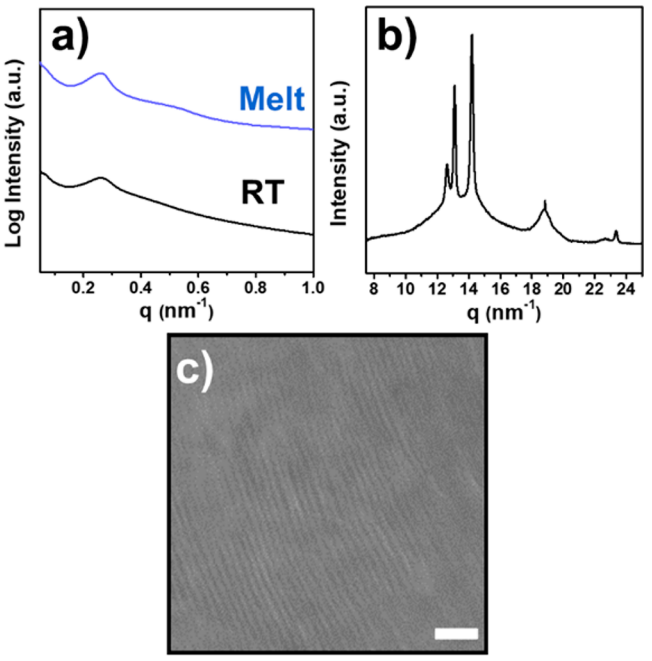

Figure 3. SAXS profiles (a), WAXS profile (b), and TEM image (c) for P2VP$_{0.17}$-*b*-PVDF$_{0.66}$-*b*-P2VP$_{0.17}$. Scale bar corresponds to 50 nm.

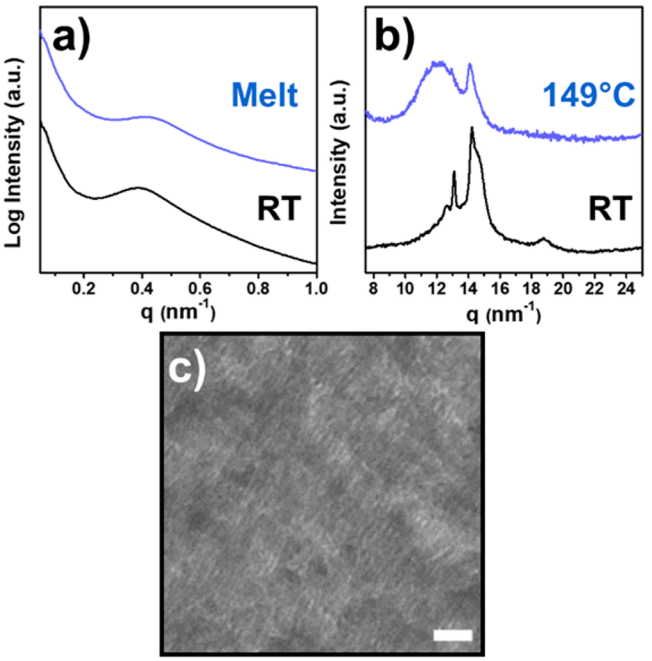

Figure 4. SAXS profiles (a), WAXS profiles (b), and TEM image (c) for P2VP$_{0.06}$-*b*-PVDF$_{0.88}$-*b*-P2VP$_{0.06}$. Scale bar corresponds to 20 nm.

see a small reduction in the crystallization temperature compared to the homopolymer, and no large undercooling is observed for P2VP$_{0.17}$-*b*-PVDF$_{0.66}$-*b*-P2VP$_{0.17}$ (Figure 2). In this case, small impurities that form nuclei that initiate crystallization are present in every lamellar domain, and therefore a heterogeneous nucleation process is observed. In the literature, similar observations are made for a large variety of block copolymer systems, such as isotactic poly(propylene)-*block*-atactic poly(styrene), poly(ethylene oxide)-*block*-poly(1,4-butadiene), and many more.[22,31] Consequently, at the crystallization temperature (128 °C) the rate of crystallization of the α-phase is highest as above-mentioned, which results in the formation of the crystalline α-phase.

In P2VP$_{0.06}$-*b*-PVDF$_{0.88}$-*b*-P2VP$_{0.06}$ the fraction of P2VP in the block copolymer is low, which leads to a disordered melt since the segregation strength (χN) between the distinct blocks is low. This is manifested in the SAXS profile in Figure 4a, wherein a correlation hole due to density fluctuations in the melt is observed. In Figure 4c, the TEM image shows that crystallization drives the self-assembly of P2VP$_{0.06}$-*b*-PVDF$_{0.88}$-*b*-P2VP$_{0.06}$ into a lamellar morphology. In addition, the POM image recorded after crystallization shows a clear birefringence pattern that is characteristic for the spherulitic superstructure.

Interestingly, the DSC scan of P2VP$_{0.06}$-*b*-PVDF$_{0.88}$-*b*-P2VP$_{0.06}$ (Figure 2) demonstrates a higher crystallization and melting temperature compared to the homopolymer PVDF. In addition, the crystallization exotherm shows a double crystallization process. To investigate the nature of the double crystallization exotherm, we recorded WAXS profiles (Figure 4b) at different temperatures during crystallization. It is observed that PVDF first crystallizes in the γ-phase, while further reduction of the temperature resulted in the α-phase formation. This is supported by the IR spectrum recorded at room temperature where the characteristic absorption bands of both the α- and γ-phase are observed (Figure S3). The γ-phase from the melt is usually obtained via slow cooling, annealing of the α-phase at high temperature, or the addition of polar fillers, such as zeolite, clay, and KBr powder.[4,32−34] It is believed that the addition of these fillers results in favorable interactions between the polar surface and PVDF chains, driving the formation of the polar γ-phase. This might explain the crystallization of PVDF into the γ-phase by interaction between the relatively polar P2VP and VDF units in the melt.

In conclusion, melt crystallization of self-assembled PVDF-based block copolymers proves to be an appealing method to study confinement effect on the crystallization mode and crystalline phases in PVDF. We show that phase behavior, crystallization mechanism, and the chemical nature of the amorphous blocks have a great impact on the crystallization behavior of PVDF in its block copolymers. The ferroelectric β-phase is formed when the crystallization of PVDF is confined in three-dimensional spherical nanodomains. Conversely, PVDF crystallization within a lamellar morphology or self-assembly due to crystallization results in the formation of the α-phase, unless favorable polar interactions between the distinct blocks during melt recrystallization initiate the formation of the polar γ-phase. These findings provide guidelines of how, in an easy way, to obtain PVDF crystalline phases desirable for advanced applications.

■ ASSOCIATED CONTENT

Supporting Information

The Supporting Information is available free of charge on the ACS Publications website at DOI: 10.1021/acsmacrolett.8b00418.

Experimental procedures, materials used, characterization details, ^{1}H NMR spectra, FTIR spectra, GPC eluograms, POM images, and the SAXS, WAXS, and TEM data for P*t*BA$_{0.3}$-*b*-PVDF$_{0.4}$-*b*-P*t*BA$_{0.3}$ (PDF)

■ AUTHOR INFORMATION

Corresponding Author

*Tel.: +31-50 363 6867. E-mail: k.u.loos@rug.nl.

DOI: 10.1021/acsmacrolett.8b00418
ACS Macro Lett. 2018, 7, 863−867

ORCID

Katja Loos: 0000-0002-4613-1159

Notes

The authors declare no competing financial interest.

■ ACKNOWLEDGMENTS

The research was supported by an NWO-VICI innovational research grant. A.J.J.Woortman is acknowledged for the GPC measurements.

■ REFERENCES

(1) Soulestin, T.; Ladmiral, V.; Dos Santos, F. D.; Améduri, B. Vinylidene Fluoride- and Trifluoroethylene-Containing Fluorinated Electroactive Copolymers. How Does Chemistry Impact Properties? *Prog. Polym. Sci.* **2017**, *72*, 16−60.

(2) Li, M.; Stingelin, N.; Michels, J. J.; Spijkman, M.-J.; Asadi, K.; Feldman, K.; Blom, P. W. M.; de Leeuw, D. M. Ferroelectric Phase Diagram of PVDF:PMMA. *Macromolecules* **2012**, *45* (18), 7477−7485.

(3) Mei, B. Z.; Scheinbeim, J. I.; Newman, B. A. The Ferroelectric Behavior of Odd-Numbered Nylons. *Ferroelectrics* **1993**, *144* (1), 51−60.

(4) Martins, P.; Lopes, A. C.; Lanceros-Mendez, S. Electroactive Phases of Poly(Vinylidene Fluoride): Determination, Processing and Applications. *Prog. Polym. Sci.* **2014**, *39* (4), 683−706.

(5) Nakagawa, S.; Marubayashi, H.; Nojima, S. Crystallization of Polymer Chains Confined in Nanodomains. *Eur. Polym. J.* **2015**, *70*, 262−275.

(6) Michell, R. M.; Blaszczyk-Lezak, I.; Mijangos, C.; Müller, A. J. Confined Crystallization of Polymers within Anodic Aluminum Oxide Templates. *J. Polym. Sci., Part B: Polym. Phys.* **2014**, *52* (18), 1179−1194.

(7) Mackey, M.; Flandin, L.; Hiltner, A.; Baer, E. Confined Crystallization of PVDF and a PVDF-TFE Copolymer in Nanolayered Films. *J. Polym. Sci., Part B: Polym. Phys.* **2011**, *49* (24), 1750−1761.

(8) Dai, X.; Niu, J.; Ren, Z.; Sun, X.; Yan, S. Effects of Nanoporous Anodic Alumina Oxide on the Crystallization and Melting Behavior of Poly(Vinylidene Fluoride). *J. Phys. Chem. B* **2016**, *120* (4), 843−850.

(9) Pan, M.; Yang, L.; Wang, J.; Tang, S.; Zhong, G.; Su, R.; Sen, M. K.; Endoh, M. K.; Koga, T.; Zhu, L. Composite Poly(Vinylidene Fluoride)/Polystyrene Latex Particles for Confined Crystallization in 180 Nm Nanospheres via Emulsifier-Free Batch Seeded Emulsion Polymerization. *Macromolecules* **2014**, *47* (8), 2632−2644.

(10) Loo, Y.-L.; Register, R. A.; Ryan, A. J.; Dee, G. T. Polymer Crystallization Confined in One, Two, or Three Dimensions. *Macromolecules* **2001**, *34* (26), 8968−8977.

(11) Müller, A. J.; Balsamo, V.; Arnal, M. L.; Jakob, T.; Schmalz, H.; Abetz, V. Homogeneous Nucleation and Fractionated Crystallization in Block Copolymers. *Macromolecules* **2002**, *35* (8), 3048−3058.

(12) Hawker, C. J.; Russell, T. P. Block Copolymer Lithography: Merging "Bottom-Up" with "Top-Down" Processes. *MRS Bull.* **2005**, *30* (12), 952−966.

(13) Bates, F. S.; Fredrickson, G. H. Block Copolymers-Designer Soft Materials. *Phys. Today* **1999**, *52* (2), 32.

(14) Widin, J. M.; Schmitt, A. K.; Schmitt, A. L.; Im, K.; Mahanthappa, M. K. Unexpected Consequences of Block Polydispersity on the Self-Assembly of ABA Triblock Copolymers. *J. Am. Chem. Soc.* **2012**, *134* (8), 3834−3844.

(15) Michell, R. M.; Müller, A. J. Confined Crystallization of Polymeric Materials. *Prog. Polym. Sci.* **2016**, *54−55*, 183−213.

(16) Loo, Y.-L.; Register, R. A.; Ryan, A. J. Modes of Crystallization in Block Copolymer Microdomains: Breakout, Templated, and Confined. *Macromolecules* **2002**, *35* (6), 2365−2374.

(17) Voet, V. S. D.; Ekenstein, G. O. R.; Meereboer, N. L.; Hofman, A. H.; Brinke, G.; Loos, K. Double-Crystalline PLLA-b-PVDF-b-PLLA Triblock Copolymers: Preparation and Crystallization. *Polym. Chem.* **2014**, *5* (7), 2219−2230.

(18) Terzić, I.; Meereboer, N. L.; Loos, K. CuAAC Click Chemistry: A Versatile Approach towards PVDF-Based Block Copolymers. *Polym. Chem.* **2018**, DOI: 10.1039/C8PY00742J.

(19) Borsboom, M.; Bras, W.; Cerjak, I.; Detollenaere, D.; Glastra van Loon, D.; Goedtkindt, P.; Konijnenburg, M.; Lassing, P.; Levine, Y. K.; Munneke, B.; et al. The Dutch−Belgian Beamline at the ESRF. *J. Synchrotron Radiat.* **1998**, *5* (3), 518−520.

(20) Bras, W.; Dolbnya, I. P.; Detollenaere, D.; van Tol, R.; Malfois, M.; Greaves, G. N.; Ryan, A. J.; Heeley, E. IUCr. Recent Experiments on a Small-Angle/Wide-Angle X-Ray Scattering Beam Line at the ESRF. *J. Appl. Crystallogr.* **2003**, *36*, 791−794.

(21) Lynd, N. A.; Hillmyer, M. A.; Matsen, M. W. Theory of Polydisperse Block Copolymer Melts: Beyond the Schulz−Zimm Distribution. *Macromolecules* **2008**, *41* (12), 4531−4533.

(22) Lin, M.-C.; Chen, H.-L.; Lin, W.-F.; Huang, P.-S.; Tsai, J.-C. Crystallization of Isotactic Polypropylene under the Spatial Confinement Templated by Block Copolymer Microdomains. *J. Phys. Chem. B* **2012**, *116* (40), 12357−12371.

(23) Gradys, A.; Sajkiewicz, P. Determination of the Melting Enthalpy of β Phase of Poly(Vinylidene Fluoride). *e-Polym.* **2013**, *13* (1), 203.

(24) Lovinger, A. J. Crystallization and Morphology of Melt-Solidified Poly(Vinylidene Fluoride). *J. Polym. Sci., Polym. Phys. Ed.* **1980**, *18* (4), 793−809.

(25) Gregorio, R. J.; Cestari, M. Effect of Crystallization Temperature on the Crystalline Phase Content and Morphology of Poly(Vinylidene Fluoride). *J. Polym. Sci., Part B: Polym. Phys.* **1994**, *32* (5), 859−870.

(26) Guo, D.; Zeng, F.; Dkhil, B. Ferroelectric Polymer Nanostructures: Fabrication, Structural Characteristics and Performance under Confinement. *J. Nanosci. Nanotechnol.* **2014**, *14* (2), 2086−2100.

(27) Hsu, C. C.; Geil, P. H. Morphology-structure-property Relationships in Ultraquenched Poly(Vinylidene Fluoride). *J. Appl. Phys.* **1984**, *56* (9), 2404−2411.

(28) Oka, Y.; Koizumi, N. Formation of Unoriented Form I Poly (Vinylidene Fluoride) by High-Rate Quenching and Its Electrical Properties. *Bull. Institute Chem. Res., Kyoto University* **1985**, *63* (3), 192−206.

(29) Coleman, M. M.; Zarian, J.; Varnell, D. F.; Painter, P. C. A Fourier Transform Infrared Study of Polymer Blends. I. Poly-(Vinylidene Fluoride) — Poly(Methyl Methacrylate) System. *J. Polym. Sci., Polym. Lett. Ed.* **1977**, *15* (12), 745−750.

(30) Shiomi, T.; Takeshita, H.; Kawaguchi, H.; Nagai, M.; Takenaka, K.; Miya, M. Crystallization and Structure Formation of Block Copolymers Containing a Rubbery Amorphous Component. *Macromolecules* **2002**, *35* (21), 8056−8065.

(31) Chen, H.-L.; Wu, J.-C.; Lin, T.-L.; Lin, J. S. Crystallization Kinetics in Microphase-Separated Poly(Ethylene Oxide)-Block-Poly-(1,4-Butadiene). *Macromolecules* **2001**, *34* (20), 6936−6944.

(32) Miyazaki, T.; Takeda, Y.; Akasaka, M.; Sakai, M.; Hoshiko, A. Preparation of Isothermally Crystallized γ-Form Poly(Vinylidene Fluoride) Films by Adding a KBr Powder as a Nucleating Agent. *Macromolecules* **2008**, *41* (7), 2749−2753.

(33) Lopes, A. C.; Costa, C. M.; Tavares, C. J.; Neves, I. C.; Lanceros-Mendez, S. Nucleation of the Electroactive γ Phase and Enhancement of the Optical Transparency in Low Filler Content Poly(Vinylidene)/Clay Nanocomposites. *J. Phys. Chem. C* **2011**, *115* (37), 18076−18082.

(34) Lopes, A. C.; Caparros, C.; Gómez Ribelles, J. L.; Neves, I. C.; Lanceros-Mendez, S. Electrical and Thermal Behavior of γ-Phase Poly(Vinylidene Fluoride)/NaY Zeolite Composites. *Microporous Mesoporous Mater.* **2012**, *161*, 98−105.

DOI: 10.1021/acsmacrolett.8b00418
ACS Macro Lett. 2018, 7, 863−867